Available online at www.sciencedirect.com
SCIENCE DIRECT
Cement and Concrete Research 35 (2005) 958–967
Cement and Concrete Research

Experimental investigation and numerical modeling of carbonation process in reinforced concrete structures Part II. Practical applications

Anna V. Saetta[a,*], Renato V. Vitaliani[b]

[a]Department of Architectural Construction, University Institute of Architecture, Venice (IUAV) 30135, Venice, Italy
[b]Department of Structural and Transportation Engineering, University of Padova, 35131, Padua, Italy

Received 5 March 2003; accepted 2 June 2004

Abstract

The mathematical–numerical method developed by the authors to predict the corrosion initiation time of reinforced concrete structures due to carbonation process, recalled in Part I of this work, is here applied to some real cases. The final aim is to develop and test a practical method for determining the durability characteristics of existing buildings liable to carbonation, as well as estimating the corrosion initiation time of a building at the design stage. Two industrial sheds with different ages and located in different areas have been analyzed performing both experimental tests and numerical analyses. Finally, a case of carbonation-induced failure in a prestressed r.c. beam is presented.

Keywords: Degradation; Carbonation; Corrosion; Durability; Modeling

1. Introduction

In Part I of this work, a brief outline of the numerical method (e.g., Refs. [1–3]) developed by the authors to provide a reliable estimation of durability performance of reinforced concrete structures subjected to carbonation process is presented together with a sensitivity analysis. This Part II describes the experimental tests and the numerical analyses performed on two industrial sheds made of the same concrete, but with different ages and located in areas with a different CO_2 content. It is an optimal opportunity to facilitate the definition of an experimental/numerical procedure for analyzing the behavior of concrete structures as concerns their degradation due to carbonation.

Subsequently, a study is presented on a case of carbonation-induced failure in a prestressed r.c. beam. First, the available data were analyzed, and then the phenomenon was numerically simulated to identify the cause and mode of failure.

Both one- and two-dimensional analyses were carried out to ascertain the effects of multidimensional attack on the concrete beam's corner reinforcing bars and to simulate all the phenomena involved in the multidimensional transport of moisture, heat and carbon dioxide through concrete. Laboratory tests were performed to determine the concrete's strength, permeability and degree of carbonation.

2. Experimental tests on two concrete structures

2.1. Introduction

The natural carbonation process in concrete has an evolution measurable in years. To obtain information on the extent of carbonation in a given construction in relation to its age, to the nature of the concrete used and to the environmental conditions, a number of specimens have to be bored from the different parts of the structure, and several measurements have to be carried out of the environmental

* Corresponding author. Dipartimento di Costruzione dell'Architettura, IUAV-Università degli Studi, Campus Terese-Dorsoduro 2206, Venezia 30123, Italy. Tel.: +39-412571311; fax: +39-415223627.
E-mail address: saetta@iuav.it (A.V. Saetta).

0008-8846/$ – see front matter © 2004 Elsevier Ltd. All rights reserved.
doi:10.1016/j.cemconres.2004.06.023

parameters (i.e., relative humidity, temperature, percentage of CO_2, etc.).

In this work, two industrial sheds similar in terms of structural type and materials involved have been analyzed. They have been built at different times, but by using prefabricated elements produced from the same supplier, who used the same mix for both the prefabricated beams with untensioned reinforcement and the columns.

The sheds are both situated in the province of Verona-Italy, in the suburbs of the city, where it is feasible to assume similar conditions in terms of the trends of temperature and relative humidity, but not of CO_2 concentrations, since one shed is used for stabling animals, the other for storing tools. Thus, the data obtained from the tests on the two sheds can be considered as representative of the "same structure" built in two different environments and at two different times. This enabled us to verify the reliability of the numerical model, which had already been tested on laboratory samples of accelerated carbonation.

First of all, a number of cores were bored in the beams and columns of the two sheds. It is worth noting that the location of cores is the same both for the beams and the columns, i.e., indoor elements.

All the fundamental parameters required for the model were directly or indirectly measured (e.g., the diffusivities were assessed by correlation with other measured properties, such as compressive strength, permeability and porosity), with the exception of the carbonation and CO_2 diffusion interaction coefficient α_3, which, as mentioned in Part I, is particularly difficult to assess.

Analyses were then performed, equating the actual carbonation depth measured on some samples made with concrete similar to the one used for the two sheds in different environments, with the carbonation depth resulting from numerical simulations obtained by varying only the coefficient α_3, in order to test the assumption that said coefficient could vary within a range of 0.4–1. The best results were found for $\alpha_3 = 0.8-1$, and thus in a field where even significant variations in the coefficient generate relatively limited differences in carbonation depth.

The main aim of these experimental/numerical analyses was to test a practical method for determining the durability characteristics of existing buildings liable to carbonation in environments that differ in terms of temperature, external relative humidity and CO_2 concentration, and to start collecting significant data relating to the concrete and the environment in order to be able, in the future, to estimate the corrosion initiation time of a building already at the design stage.

In addition to the age of the concrete, the so-called *fundamental* parameters that most affect carbonation depth d_c are as follows: the diffusivity of humidity and CO_2 in the material (C and D_c), the ratio between the values of these diffusivities at infinity and at 28 days (χ), and the carbonation and gas diffusion interaction coefficient (α_3). More than the parameters relating to the concrete, the model also considers the environmental conditions, i.e., the external volumetric fraction of the diffusing specie CO_2 (g_{env}), the relative humidity (h_{env}), and the temperature (T_{env}). Briefly, we can thus write:

$$d_c = d_c(t, C, D_c, \chi, \alpha_3, g_{env}, h_{env}, T_{env}) \quad (1)$$

2.2. Environmental parameters

Measuring environmental parameters, such as the CO_2 concentration, the presence of sulfates and the relative humidity, is essential to classify the aggressive potential of the environmental context of a given building. Urban, industrial and rural environments are characterized by different environmental parameter sets that must be known, or predicted on the strength of experimental data, for the correct design of a building's durability.

The concrete elements which have been analyzed are indoor elements, but due to the use of the sheds, they are subjected to wetting (by condensation) and drying cycles. Such a condition has been simulated in a simplified way by assuming a variable boundary condition both for environmental humidity and temperature (see Section 3.1–Table 3).

Together with these environmental parameters, there are also those depending on the type of concrete. The influence that each parameter used as input for the model has on carbonation depth has been discussed in the Part I of this work.

The concentration of CO_2 in the air is one of the fundamental environmental parameters that most affects the rate of carbonation and can be considered as one of the parameters defining the aggressiveness of the environment.

In the present research, CO_2 concentrations were measured in the open country, in the city, in the industrial zone and in several stables.

The CO_2 values measured in these environments, in terms of volumetric concentration, are given in Table 5 of the Part I of the present paper.

The concentration assumed in the simulations for shed A was 0.075% for the "low-aired stable", while the 0.015% recorded for the "open country" was used for the tool shed (Shed B). Fig. 1 shows the *chromatograms* obtained by analyzing the air coming from the two environments considered. Such a diagram has been obtained by the technique of gas chromatography, which is a technique used for separating volatile substances from one another in a gaseous mixture, with thermal conductivity detector. The sample of air to be separated is injected into the gas chromatograph to separate carbon dioxide, nitrogen and oxygen. Each of such gases has an influence on the thermal conductivity of the packed column, proportional to the concentration, but in different times.

2.3. Concrete parameters

To characterize the mechanical properties of the concrete, cores were bored in both sheds in order to establish

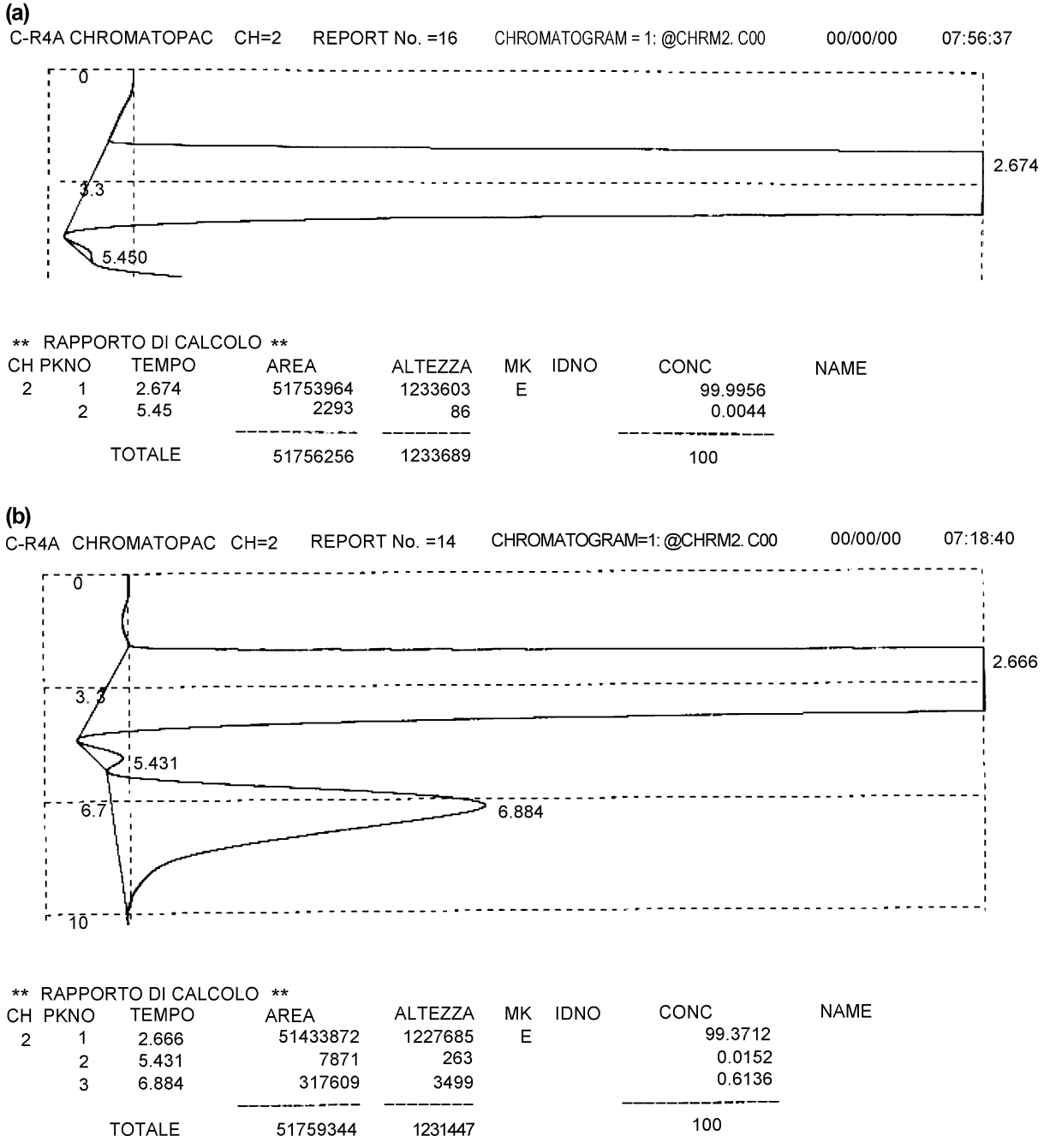

Fig. 1. Chromatograms: (a) open country—Shed B, (b) low-aired stable—Shed A.

the carbonation depth, compressive strength, porosity and permeability of the concrete. The test methods used to determine each fundamental parameter are described in detail below.

2.3.1. Experimental determination of the carbonation depth in the concrete

One of the effects of carbonation is to reduce the alkalinity of the water solution in the concrete, changing the pH from around 12 (typical of intact concrete) to around pH 8.3, which is characteristic of carbonated concrete.

One of the most common methods for testing the carbonation depth consists in spraying a sample cross-section, i.e., a section parallel to the direction of carbonation, with a pH indicator. In the case in point, a 1–2% water–alcohol solution of phenolphthalein was used, which produces a pink stain (typical of phenolphthalein in an alkaline medium) in areas with a pH higher than 9, while the areas with a pH < 9 (where carbonation has occurred) remain colorless.

Actually, the carbonation process is more complex than described by such a simple method, and it is difficult to

Table 1
Specimen characteristics and results of ultimate compressive strength tests

Shed	Specimen	Diameter, d (mm)	Height, h (mm)	h/d	Area A (mm^2)	$F_{failure}$ (kN)	S (MPa)	R_c (MPa)	f_c (MPa)
A	T2-4	44	83	1.91	1486	67.4	45.4	56.0	44.8
A	T3-5	44	82	1.90	1486	62.6	42.1	52.0	41.6
					Mean values	65.0	43.7	54.0	43.2
B	P1-1A	44	89.0	2.05	1486	57.2	38.5	48.4	38.7
B	P1-2	44	87.3	2.01	1486	60.2	40.5	50.7	40.5
					Mean values	58.7	39.5	49.5	39.6

identify the carbonation depth with a precise number [4]. Usually, three zones can be distinguished: the first one, which is close to the external surface, is fully carbonated; the second one, the so-called "carbonation front", is a transition zone where the degree of carbonation decreases gradually to zero; finally, the third zone is not carbonated at all.

As stated in Ref. [4], there is no simple correlation between measurements of carbonation depth as determined after phenolphthalein test and the actual profiles of carbonate content. In such a work, on the same mortars, the authors have found that the measured carbonation depth corresponds to rather different carbonate contents, even if part of these differences could be due to the variability of the carbonation front measured after phenolphthalein spraying and which should be indicated with a standard deviation.

In the beams belonging to Shed A and in the columns belonging to Shed B, the carbonation depth was measured by spraying a solution of 1% phenolphthalein directly onto the outer surface of each core. The total number of cores was 12 for the beams and 10 for the columns and such cores were obtained with almost dry cutting technique. With the aid of a gauge, four readings ($d_{c1},\ldots,d_{c4}$) were taken for each face and the mean value (d_{cm}) was assumed to be representative of the carbonation on the face concerned. These values were then further averaged, and the standard deviation has been evaluated:

- in the shed used for stabling animals, the average carbonation depth was 11.2 mm after 16 years of service, and the standard deviation, determined from average readings from all cores, is 1.75.
- in the tool shed, it was 7.1 mm after 23 years, and the standard deviation is 1.01.

In both sheds, the surface of the cores had a smooth and homogeneous appearance, with no clumps of gravel, suggesting that the elements analyzed had been correctly prepared using concrete that was not too wet, and correctly vibrating the still plastic mixture.

Moreover, from the measures carried out for the carbonation depth, even if with a limited standard deviation, it is very difficult to identify a precise number. Therefore, in the comparison with the numerical results, the obtained mean values have been rounded to the nearest 0.5 mm: 11 and 7 mm, respectively, for Shed A and Shed B.

2.3.2. Compressive strength

For each shed, a number of cores were collected and submitted to ultimate compressive strength tests to investigate the concrete's strength. Table 1 summarizes the dimensions of the specimens and the results of the compressive test in term of maximum force F ($F_{failure}$)

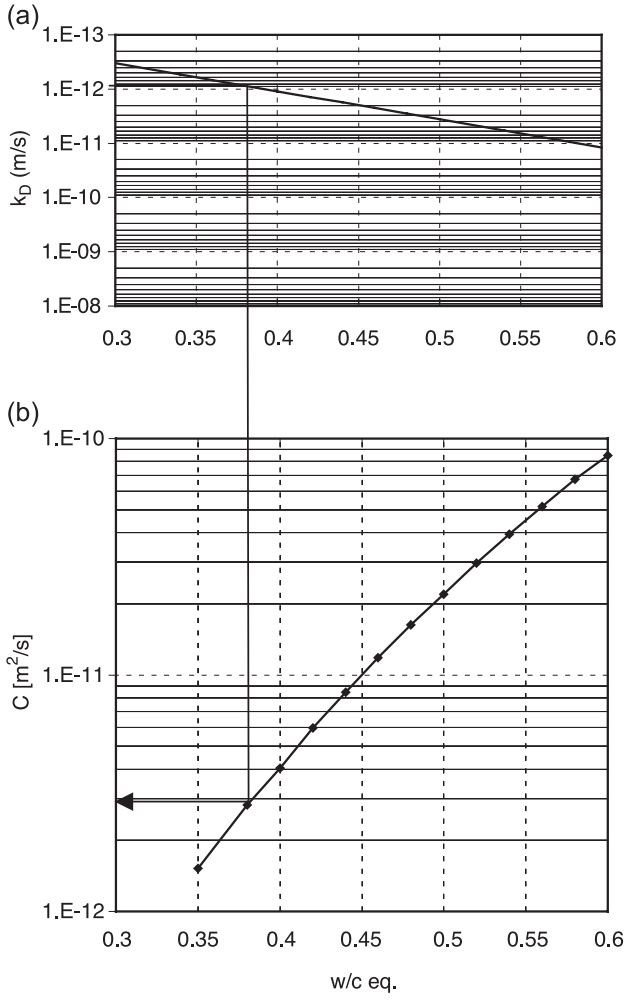

Fig. 2. Diagrams: (a) w/c – coefficient of concrete permeability, (b) humidity diffusivity – w/c.

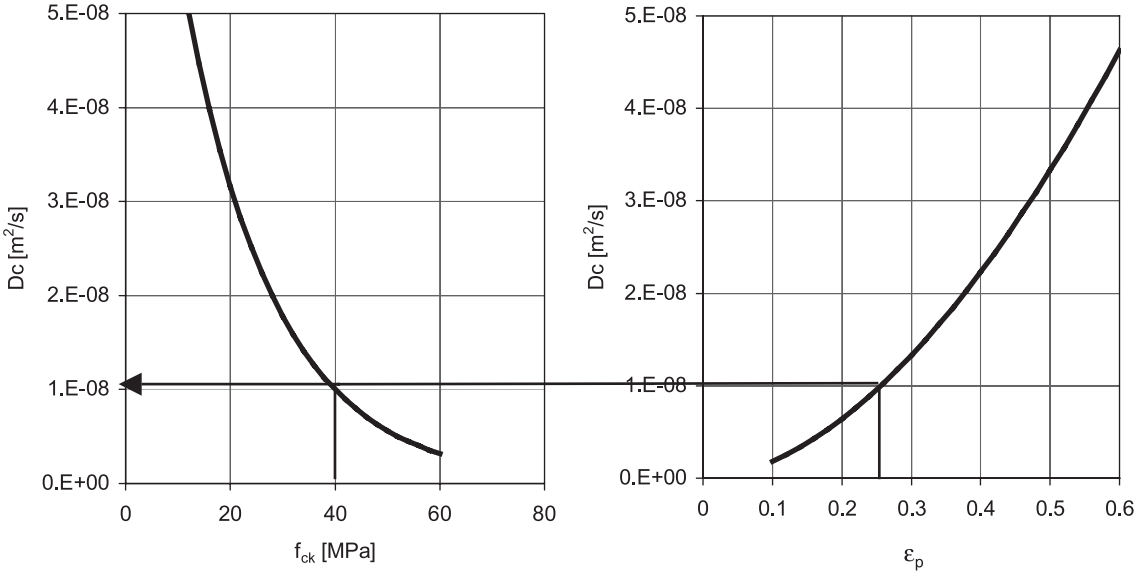

Fig. 3. Assessment of CO_2 diffusivity.

applied by the test press, specimen strength (S), cubic compressive strength (R_c) and cylindrical compressive strength (f_c). The relationship used to estimated R_c from S is based on the relationship suggested by the BS 6089:1981 standard:

$$R_c = \frac{K}{1.5 + \frac{d}{h}} \times S$$

where K is assumed 2.5, d and h are, respectively, the diameter and the height of the specimen (Table 1). It is worth noting that such a value represents the cubic strength at the time of the test.

Finally, the ratio between f_c and R_c is assumed equal to 0.8, according to the European standard for concrete of class C40/50 (see Table 3.1 of Ref. [5]).

This test revealed a substantial homogeneity of the concrete used in Sheds A and B. The mean cylinder strength was 43 MPa for Shed A and 40 MPa for Shed B. It was consequently assumed that both sheds have been built by using concrete of class C40/50.

2.3.3. Porosity

The porosity, i.e., the ratio of the volume of cavities to the total volume of the concrete, was measured by first saturating four concrete samples, by leaving them immersed in water for several days until they reached a constant saturated mass, then drying them in the oven at a temperature 105 ± 5 °C until they reached a constant dry mass.

This gave us the volumetric mass in saturated and dry conditions, the mass absorption and the porosity for each sample. The mean porosity values measured in the two sheds were virtually the same, amounting to about 15%, with standard deviation of 0.7.

2.3.4. The permeability coefficient according to Valenta

The permeability coefficient (k_D) was measured according to the *Valenta method* (e.g., Ref. [6]), by using four specimens for both the beams and the columns.

Each permeability test lasted about 10 days and the average results for the two sheds were very similar, i.e., 8.3e − 13 m/s for Shed A and 9.4e − 13 m/s for Shed B, confirming the excellent features of the concrete involved.

2.3.5. Indirect measurement of the humidity diffusivity

Whatever the composition and characteristics of the concrete, measuring its permeability enables us to establish the conventional w/c ratio and thus the diffusivity to adopt in the numerical simulation.

Table 2
Determination of the CO_2 diffusion coefficient starting from concrete mass absorption measurements

Concrete sample from	Mass absorption of concrete ε [%]	Concrete porosity [%]	a/c	w/c	ρ_c [g/cm^3]	ρ_a [g/cm^3]	Mass absorption of cement paste, ε_p [%]	Relative humidity [%]	$D_c(h)$ [m^2/s]	D_c CEB-FIP [m^2/s]
Shed A	6.75	15.13	6	0.38	3.15	2.65	28.7	70	1.2e − 08	1.00e − 08
								72.5	1.0e − 08	
								75	8.2e − 09	
Shed B	6.98	15.24	6	0.38	3.15	2.65	29.6	70	1.3e − 08	
								72.5	1.1e − 08	
								75	8.7e − 09	

Table 3
Numerical parameters for the concrete and environmental conditions for both sheds

Shed	C (m^2/s)	D_c (m^2/s)	D_∞/D_{28}	α_3	Temperature, T_{env} (°C)	Relative humidity, h_{env} (%)	CO_2 (%)
A	3.0e − 12	1.0e − 8	0.8	0.8–1	5–25	$75 + 15 \cdot \cos\left(\frac{t(h)}{8760} \cdot 2\pi\right)$	0.075
B	3.0e − 12	1.0e − 8	0.8	0.8–1	5–25	$75 + 15 \cdot \cos\left(\frac{t(h)}{8760} \cdot 2\pi\right)$	0.015

Fig. 2 shows the diagram that correlates the w/c ratio with the concrete permeability coefficient (see Ref. [7]) and the trend of the humidity diffusivity as a function of the w/c ratio (diagram obtained by interpolating the experimental results provided by the Federal Polytechnic of Zurich).

In combination, the two diagrams form a practical nomogram that enables the humidity diffusion coefficient to be ascertained from the permeability value.

In the case in point, given the measured permeability coefficients, the concrete was found to have a w/c ratio of 0.38, which coincided with a value of $C = 3 \times 10^{-12}$ m^2/s.

2.3.6. Indirect measurement of the CO_2 diffusivity

A crossover method was used to determine the diffusivity coefficient for the CO_2, starting from the known cylinder strength and the measurement of the mass absorption of the concrete (see Fig. 3).

From the mass absorption of the concrete (ε), the mass absorption of the cement paste contained in the concrete (ε_p) was established by means of the formula:

$$\varepsilon_p = \varepsilon \times \left(1 + \frac{\frac{a}{c} \cdot \frac{\rho_c}{\rho_a}}{1 + \frac{w}{c} \cdot \frac{\rho_c}{\rho_w}} \right) \quad (2)$$

where w/c is the water/cement ratio, a/c the mass aggregate/cement ratio, and ρ_c, ρ_w and ρ_a the volumetric mass of the cement, water and aggregate.

Once ε_p is known, the CO_2 diffusivity is determined using the formula proposed in Ref. [8]:

$$D_c \left[\frac{m^2}{s} \right] = 1.64 \times 10^{-6} \times \varepsilon_p^{1.8} \times \left(1 - \frac{RH}{100} \right)^{2.2} \quad (3)$$

The results are given in Table 2 for an RH varying between 70% and 75%.

The concrete strength class in question is C 40/50; thus, based on Ref. [9], we shall have:

$$D_c = 10^{-7} \times 10^{-0.025 \cdot f_{ck}} = 1 \times 10^{-8} \ m^2/s \quad (4)$$

Such a value coincides with the result derived from the measurement of the concrete's mass absorption and is the one adopted in the numerical simulations.

3. Numerical tests on two concrete structures

3.1. Assumption of the fundamental parameters

Based on the results of the tests, Table 3 shows the characteristic parameters relating to the concrete of both sheds and the environmental parameters adopted in the numerical models. The only parameter for which some additional considerations have to be included is the carbonation and CO_2 diffusion interaction coefficient α_3. According to what previously stated (Section 2.1), such a coefficient α_3, for the specific concrete of which the two shed are made, varies between 0.8 and 1. In order to explore how such a variability influences the results in such an example, several analyses have been carried out by varying only the parameter α_3 between 0.8 and 1. The results demonstrate that in such a range, no significant differences in carbonation depth have been obtained; therefore, in the following analyses, it was assumed that $\alpha_3 = 0.8$.

3.2. Numerical carbonation tests

Numerical simulations of the progression of the carbonation front were done for both sheds. Fig. 4 shows the carbonation-depth/time diagrams for the two different environments. These graphs demonstrate a good consistency

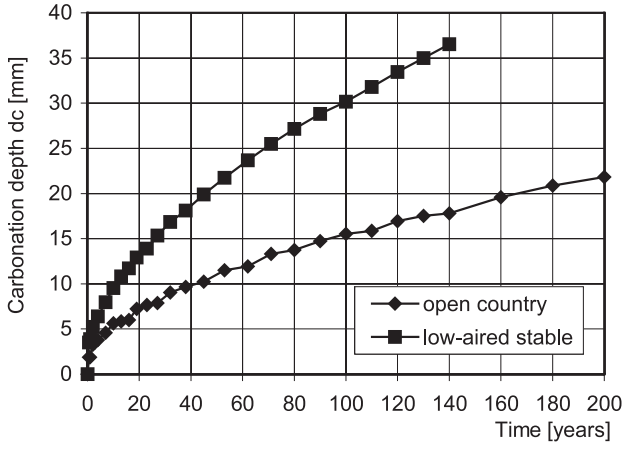

Fig. 4. Carbonation-depth/time diagrams for the two different environments.

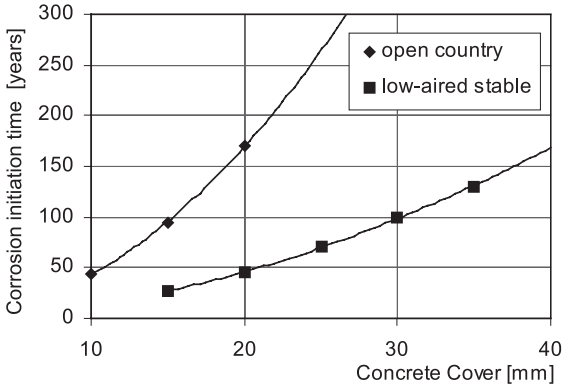

Fig. 5. Corrosion initiation time in relation to concrete cover thickness for the two different environments.

between the experimental findings and the numerical model:

- for Shed A, an experimentally measured carbonation depth of about 11 mm after 16 years of service agrees with the value of depth obtained by the model, which is between 11 and 12 mm;
- for Shed B, the experimental finding was about 7 mm after 23 years, while the simulated result is between 7 and 8 mm.

Table 4
Prestressed beam—compressive strength

Specimen number	Cube strength (MPa)	Cylinder strength (MPa)
4	39.0	31.2
6	43.5	34.8
11	39.0	31.2
12	37.2	29.8
14	35.4	28.3
Mean values	**38.8**	**31.0**

In terms of corrosion initiation time, Fig. 5 shows the results of the numerical simulation for different thicknesses of concrete cover in both the environments considered.

4. Failure of a prestressed concrete beam

The last application of the numerical model presented here concerns the study of a prestressed beam that collapsed due to corrosion of the reinforcement bars. This beam belonged to an industrial shed also situated in the province of Verona-Italy, where the environmental conditions (temperature and humidity) were much the same as those described in the previous section.

The prestressed concrete beam of the industrial shed (i.e., a store for cereal and fodder) suddenly collapsed after only

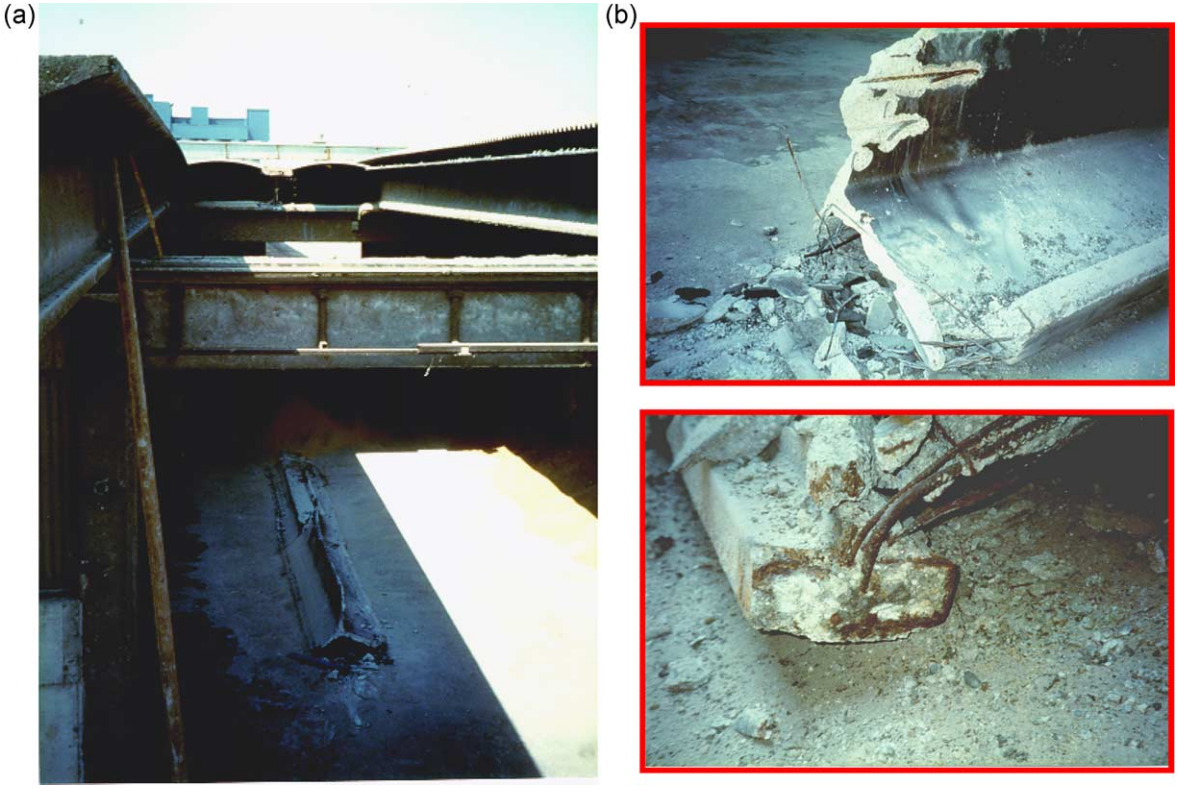

Fig. 6. (a) Collapsed prestressed concrete beam (b) Critical section of beam.

Table 5
Prestressed beam—carbonation depth

Specimen number	Carbonation depth (mm)
8	21.5
T1	20.7
TR	24.7
TR	23.3
Mean values	**22.5**

Table 6
Prestressed beam—parameters assumed in the numerical simulation

Numerical parameter		Value
Concrete		
Diffusivity of relative humidity	C	3.0e − 12 m^2/s
Diffusivity of carbon dioxide	D_c	1.8e − 8 m^2/s
Cement hydration coefficient	$\chi = D_\infty/D_{28}$	0.8
Coefficient of interaction between carbonation and CO_2 diffusivity	α_3	0.8
Environment		
CO_2 concentration	g_{env}	0.1%
Relative humidity	h_{env}	0.75
Temperature	T_{env}	20 °C

17 years of service: the shed was built in 1980 and its failure occurred in 1997.

The beam is a "Y" beam, 90 cm high. The static arrangement is a simply supported beam with a span of 16.8 m and a cantilever of 5 m.

Fig. 6a shows the beam after failure, laid on the floor of the shed. Fig. 6b shows the critical section of the collapsed beam, with evidence of the complete corrosion of the reinforcing bars.

Experimental and numerical investigations were carried out to establish why the beam failed.

4.1. Experimental measurements

Experimental tests were carried out on specimens collected both from the collapsed beam and from other intact beams in the shed. The aim was to assess the mechanical and technological characteristics of concrete as well as the carbonation depth. In particular, even if the failure is obviously due to the underside of the beam as clearly demonstrated in the following, the carbonation measurements have been taken from all the sides of the beam, i.e., web and underside, in order to have a complete outline of the carbonation process, which is effective in the identification of the cause and mode of the failure. Moreover, the web measurement provides a reference value of carbonation depth, which is not influenced by failure phenomena or bidimensional effects (i.e., corner effect), which will be used to check the results obtained by applying the proposed numerical model.

Table 4 summarizes the results of compressive strength tests carried out on the concrete specimens. The concrete was assumed to belong to the strength class C 30/37.

Similarly, Table 5 shows the carbonation depth measured in several specimens extracted from the left and right sides of the web of the beam. The mean value is equal to 22.5 mm.

The carbonation depth was also measured on the underside of the collapsed beam. Fig. 7 shows the carbonation in the critical section (where the carbonation front has reached the reinforced concrete's prestressing strand), and in an intact section.

The carbonation measured on the underside of the collapsed beam proved to be three times deeper than in the web of the beam. This could be due to a greater porosity of concrete in this part of the section than in the web, but also to the possibility that in the lower part of the beam, the effect of drying is more significant. Finally, in such a zone, the effect of a bidimensional flux of carbon dioxide is not negligible (i.e., the so-called corner effect).

It is worth noting that in the collapsed beam (Fig. 7a), the carbonation depth varied over a significant range, with certain parts of the flange showing zero value. In particular, the left side of the flange has very low carbonation compared to the right side, and this could be due to the

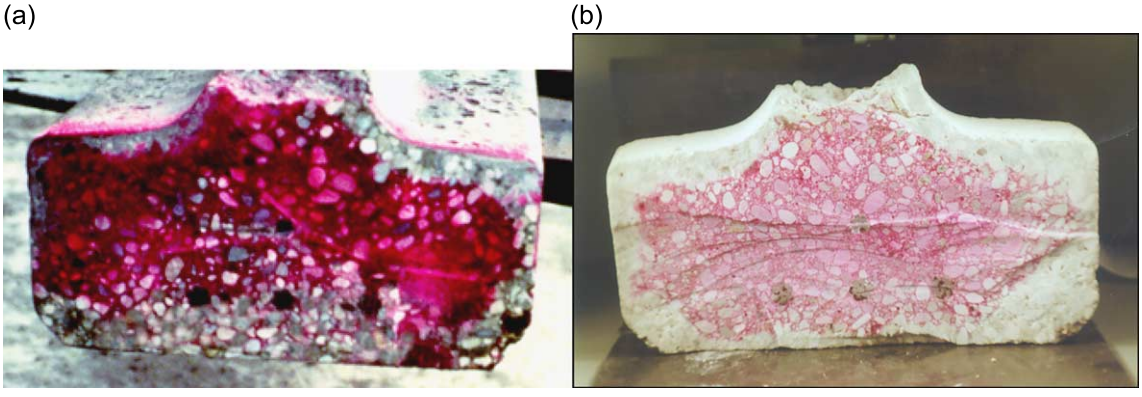

Fig. 7. Experimental assessment of carbonation depth: (a) unprotected bars (b) protected bars.

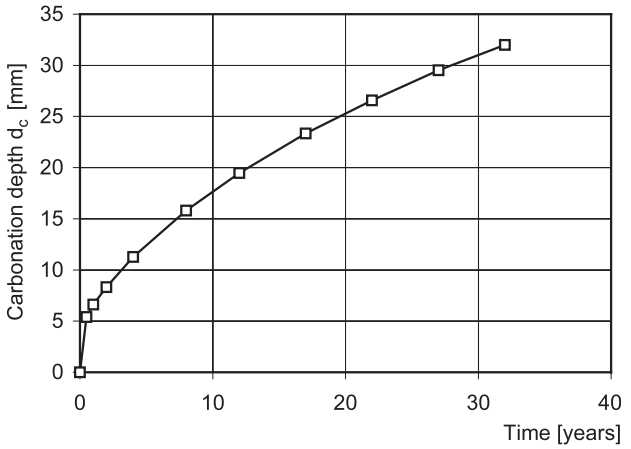

Fig. 8. 1-D numerical simulation: carbonation depth versus time, assuming $g_{env} = 0.1\%$.

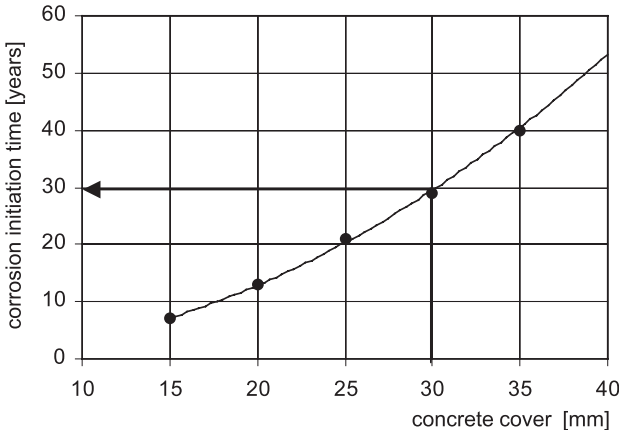

Fig. 10. 2-D numerical simulation: corrosion initiation time–concrete cover diagram.

location of the beam, the left side being more protected by drying effects, or to some local effects.

4.2. Numerical simulation

The numerical model recalled in Part I of this work was applied to simulate the propagation of carbon dioxide inside the beam and to predict the evolution of the carbonation process.

First of all, a one-dimensional simulation was used to test the parameter assumed for the concrete's characteristics and the environmental conditions. The finite element mesh adopted consists of 20 elements 2 mm long (total length 40 mm). Table 6 summarizes the parameters assumed in the numerical simulation.

Fig. 8 shows the results of the numerical analysis in terms of carbonation depth versus time, assuming $g_{env} = 0.1\%$. The carbonation depth after 17 years amounts to 23 mm, which was consistent with the experimental findings obtained on the specimens taken from the web of the beam.

After this parameter calibration phase, performed using both the experimental data and one-dimensional analyses for simulating the web's behavior, a two-dimensional analysis of the lower part of the beam was carried out.

Fig. 9a shows the finite element mesh used in this 2-D numerical simulation, while Fig. 9b depicts the carbonation front. It is worth noting the corner effect due to the multidimensional attack on the concrete structures, which makes the carbonation front more advanced near the corners C and D (i.e., the convex zones), due to the effect of two-dimensional flow. The difference in penetration between the mono- and two-dimensional diffusion processes can be estimated at approximately 40%.

Conversely, near corners A and B, which are concave zones, the lesser carbonation depth is due to the fact that the concrete surface in direct contact with environment is smaller. This result is consistent with the experimental evidence shown in Fig. 7b. However, it is worth noting that the numerical simulation is not able to take into account the imperfections and the nonsymmetric response of the beam evidenced by the experimental picture. As an example, the numerical model is not able to pick up the difference between the carbonation depth in the right and left sides (see Fig. 7b), which can be due to difference in environmental conditions, but more probably to some local effect.

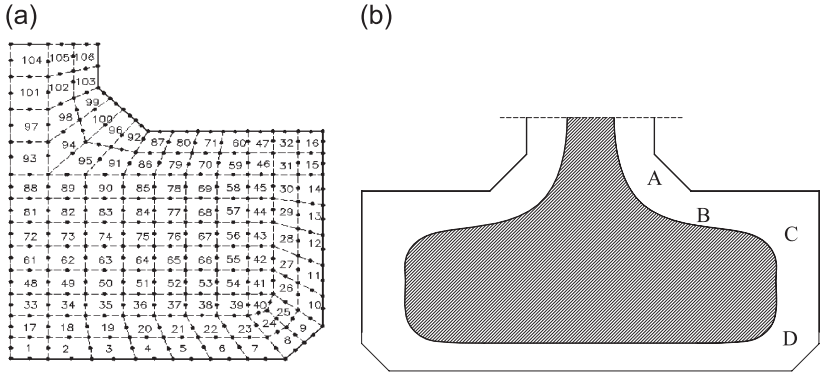

Fig. 9. 2-D numerical simulation: (a) finite element mesh (b) carbonation front.

The failure seems due to localized corrosion of the reinforcing bars in the critical section of the collapsed beam, since the bars in the remainder the collapsed beam were still protected by an alkaline environment, i.e., the carbonation front had not yet reached the bars. This is also demonstrated by the numerical results of 2-D simulations that provide a corrosion initiation time of about 29–30 years (see Fig. 10), while the actual age of the building at the time of failure was 17 years.

The high level of carbonation in the critical section was consequently attributed to a local material defect, i.e., a segregation process and gravel accumulation. Such a hypothesis was also supported by the visual analyses on the concrete in the critical section.

5. Conclusions

The model presented in Part I of this work for simulating the carbonation process enables the influence of the various parameters involved to be considered in the governing equations.

To demonstrate the potential of the model for predicting the corrosion initiation time of r.c. structures, two industrial sheds suffering from carbonation phenomena were studied performing both experimental tests and numerical analyses. Finally, a case of prestressed concrete beam failure was investigated.

Acknowledgement

We wish to thank ing. Giovanni Pezzini for his contribution in testing the model and developing the numerical examples during the preparation of his degree thesis.

Appendix A. List of symbols

The following symbols are used in this paper:

a/c	Ratio between mass aggregate and cement
C	Relative humidity diffusion coefficient
d_c	Carbonation depth
D_c	Aggressive specie diffusion coefficient
f_c	Cylindrical compressive strength
g_{env}	External volumetric fraction of the diffusing specie CO_2
h_{env}	Environmental relative humidity
k_D	Permeability coefficient
R_c	Cubic compressive strength
S	Specimen strength
t	Time
T_{env}	Environmental temperature
w/c	Ratio between water and cement
α_3	Parameter which accounts for the possible interaction between the pollutant flow and the chemical reaction
ε	Mass absorption of the concrete
ε_p	Mass absorption of the cement paste contained in the concrete
χ	Cement hydration coefficient: ratio between the diffusion coefficient for te $\rightarrow \infty$ and for te = 28 gg
ρ_c	Volumetric mass of the cement
ρ_w	Volumetric mass of the water
ρ_a	Volumetric mass of the aggregate

References

[1] A., Saetta, Durabilità delle strutture di calcestruzzo armato e analisi dei fenomeni di diffusione dei materiali multifase, PhD dissertation, Padova 1992.
[2] A.V. Saetta, B.A. Schrefler, R.V. Vitaliani, The carbonation of concrete and the mechanism of moisture, heat and carbon dioxide flow through porous materials, Cem. Concr. Res. 23 (4) (1993) 761–772.
[3] A.V. Saetta, B.A. Schrefler, R.V. Vitaliani, 2-D Model for carbonation and moisture–heat flow in porous materials, Cem. Concr. Res. 25 (8) (1995) 1703–1712.
[4] Y.F. Houst, F.H. Wittmann, Depth profiles of carbonates formed during natural carbonation, Cem. Concr. Res. 32 (2002) 1923–1930.
[5] UNI ENV 1992-1-1 (Eurocodice 2)-31/01/1993-Eurocodice 2. Progettazione delle strutture di calcestruzzo. Parte 1-1: Regole generali e regole per gli edifici, Unistore, Codice ICS: 91.080.40, UNI-Ente Nazionale Italiano di Unificazione, Milano.
[6] O. Valenta, Kinetics of water penetration into concrete as an important factor of its deterioration and of reinforcement corrosion, RILEM International Symposium: Durability of Concrete —1969, Part 1, RILEM Publications, Prague, 1969, pp. A177–A189.
[7] Concrete Manual, 8th ed., Denver, Colorado, 1975. A Water Resources Publication, U.S. Department of the Interior, Bureau of Reclamation, 1975.
[8] V.G. Papadakis, C.G. Vayenas, M.N. Fardis, Physical and chemical characteristics affecting the durability of concrete, ACI Mater. J. 88 (2) (1991) 86–196.
[9] CEB-FIP Model Code, Section 2.1.9., Transport of Liquids and Gases in Hardened Concrete, Thomas Telford London, United Kingdom, 1990.